Search for the Rare Decay $\mu^+ \rightarrow e^+\gamma\gamma$

D. Grosnick and S. C. Wright
University of Chicago, Chicago, Illinois 60637

R. D. Bolton, M. D. Cooper, J. S. Frank, A. L. Hallin,[a] P. A. Heusi,[b] C. M. Hoffman, G. E. Hogan, F. G. Mariam, H. S. Matis,[c] R. E. Mischke, L. E. Piilonen, V. D. Sandberg, G. H. Sanders, U. Sennhauser,[d] R. Werbeck, and R. A. Williams
Los Alamos National Laboratory, Los Alamos, New Mexico 87545

S. L. Wilson,[e] R. Hofstadter, E. B. Hughes, and M. W. Ritter[f]
Hansen Laboratories and Department of Physics, Stanford University, Stanford, California 94305

and

V. L. Highland and J. McDonough
Temple University, Philadelphia, Pennsylvania 19122
(Received 15 August 1986)

A new experimental search with the Crystal Box detector shows no evidence for the lepton-family-number–nonconserving decay $\mu^+ \rightarrow e^+\gamma\gamma$. This corresponds to an upper limit for the branching ratio of $\Gamma(\mu \rightarrow e\gamma\gamma)/\Gamma(\mu \rightarrow e\nu\bar{\nu}) < 7.2\times10^{-11}$ (90% confidence level), an improvement of more than 2 orders of magnitude in sensitivity.

PACS numbers: 13.35.+s, 11.30.Er

Neutrinoless muon decays, such as $\mu^+ \rightarrow e^+\gamma\gamma$, do not conserve lepton-family number and are not allowed in the minimal standard model of electroweak interactions.[1] Many extensions to the standard model include the nonconservation of lepton-family number. In several of these extensions,[2] the branching ratio for $\mu^+ \rightarrow e^+\gamma\gamma$ limits model parameters and some models[3,4] predict a larger rate for $\mu^+ \rightarrow e^+\gamma\gamma$ than for $\mu^+ \rightarrow e^+\gamma$.

The best published experimental upper limit for this decay mode is[5]

$$B_{\mu e\gamma\gamma} \equiv \frac{\Gamma(\mu^+ \rightarrow e^+\gamma\gamma)}{\Gamma(\mu^+ \rightarrow e^+\nu_e\bar{\nu}_\mu)} < 8.4\times10^{-9}$$ [90% confidence level (C.L.)].

We report here a new upper limit for $B_{\mu e\gamma\gamma}$ using data obtained with the Crystal Box detector. This detector, located in the stopped-muon channel at the Clinton P. Anderson Meson Physics Facility (LAMPF), searched simultaneously for the decays $\mu^+ \rightarrow e^+e^-e^+$,[6] $\mu^+ \rightarrow e^+\gamma$,[7] and $\mu^+ \rightarrow e^+\gamma\gamma$. This is the first $\mu^+ \rightarrow e^+\gamma\gamma$ experiment to use a detector with a large solid-angle acceptance and to observe all three final-state particles separately.

The Crystal Box detector[6] encloses a thin polystyrene target with a high-resolution cylindrical drift chamber, a 36-element plastic scintillator hodoscope, and 396 NaI(Tl) crystals arranged in four quadrants. Positive muons from a separated, 26-MeV/c beam decay at rest in the target. The typical muon stopping rate is 4×10^5 s^{-1} (average) with a beam duty factor from 5% to 10%. Energy measurements for positrons and photons show a resolution of 8% (FWHM) at 50 MeV in the NaI(Tl). Photon time signals are measured in the NaI(Tl) with a resolution of 1.2 ns (FWHM) for photon energies above 28 MeV. The resolution is slightly worse for energies below 28 MeV. Positron time signals from the plastic scintillators show a resolution of 290 ps (FWHM). The drift chamber determines the intersection point of the target plane with the positron trajectory within 2 mm. Each photon trajectory is assumed to originate from this point. The photon conversion point in the NaI(Tl) array is found by an energy-weighted average of the NaI(Tl) crystal positions for those crystals in which more than 5 MeV is deposited. The position resolution of the conversion point is 4.1 cm (FWHM).

The signature for $\mu^+ \rightarrow e^+\gamma\gamma$ at rest is (1) a positron and two photons in time coincidence, (2) the sum of the energies of the three particles equal to the muon mass, and (3) the vector sum of the momenta of these particles equal to zero. The trigger is based on the four quadrants of NaI(Tl) crystals and the scintillators in front of each quadrant. A "positron quadrant" is a quadrant with a scintillator signal and at least 5 MeV of energy deposited in the NaI(Tl) crystals for that quadrant. A "photon quadrant" is a NaI(Tl) quadrant containing at least 5 MeV and no discriminator signal from scintillators for that quadrant. The $e\gamma\gamma$ trigger requirements are (1) only one positron quadrant, (2) at least two photon quadrants in addition to the positron quadrant, and (3) at least 70 MeV deposited in the entire NaI(Tl) array. The positron and photon signals must be within 12 ns.

© 1986 The American Physical Society

These trigger requirements exclude events containing two of the three particles in the same quadrant. Two-quadrant $e\gamma\gamma$ events may satisfy the $e\gamma$ trigger, which is (1) one positron quadrant with at least 30 MeV deposited in its NaI(Tl) crystals and (2) one photon quadrant, opposite the positron quadrant, with at least 30 MeV deposited in the NaI(Tl) crystals.

There are 2.2×10^6 three-quadrant $e\gamma\gamma$ candidate events and 1×10^5 two-quadrant $e\gamma\gamma$ candidate events satisfying the $e\gamma$ trigger requirements. Restrictions on the energy, time spread, and geometry, to satisfy $\mu^+ \rightarrow e^+\gamma\gamma$ kinematics at the 5σ level, remove 98% of the triggers during the initial analysis of the data. Also, two-quadrant $e\gamma\gamma$ candidate events with both photons in the same quadrant are rejected because most of these events have a single photon misidentified as two separate photons. This topology is not favored for an $e\gamma\gamma$ event according to particle position distributions calculated from the most general local interaction.[4] Neglect of these events eliminates 16% of the candidate events with only a 1% loss in detector acceptance for $\mu^+ \rightarrow e^+\gamma\gamma$.

An identification of the background processes can be made from Fig. 1, a plot of the time of the photons relative to the positron. The higher-energy photon is labeled γ_1 and the lower-energy photon, γ_2. The data displayed in Fig. 1 include an additional constraint that the angle between the two photons be greater than 40°. This constraint is used only in this plot to show clearly the different types of background processes: It is not used in the data analysis. The diagonal band primarily corresponds to events with a positron in coincidence with a single photon that is misidentified as two separate, time-correlated photons. This misidentification is due mainly to secondary photons, produced in the electromagnetic shower of the primary photon within the NaI(Tl), that emerge from the front face of the NaI(Tl), traverse some distance in air, and enter the crystals of a different quadrant. The horizontal and vertical bands consist of positron and photon coincidences, which are mostly muon inner-bremsstrahlung decays, $\mu^+ \rightarrow e^+\nu_e\bar{\nu}_\mu\gamma$, in random coincidence with a photon. Events scattered uniformly over the plot are random coincidences of the three particles. The central region is comprised of positron and two photon coincidences, which are combinations of the above backgrounds plus any $\mu^+ \rightarrow e^+\gamma\gamma$ events.

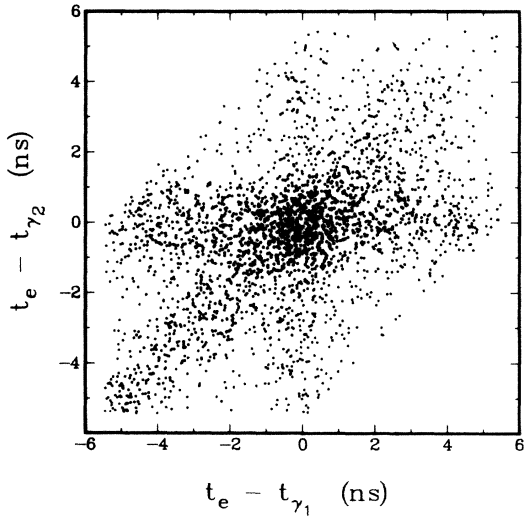

FIG. 1. Plot of the time differences between the positron and the higher-energy photon (γ_1), $t_e - t_{\gamma_1}$, and the positron and the lower-energy photon (γ_2), $t_e - t_{\gamma_2}$. An additional cut requiring that the angle between the two photons be greater than 40° is imposed to show the different background processes clearly.

From the kinematics of the $\mu^+ \rightarrow e^+\gamma\gamma$ decay, the sum of the energies from any two of the three particles must be at least one-half the muon mass. Each two-particle energy sum is required to greater than 51 MeV. In addition, the photon energies are required to be greater than 20 MeV. The latter requirement separates background from $\mu^+ \rightarrow e^+\gamma\gamma$ events, which have a small probability of containing photons with low energies.[4] A total of 364 events pass these cuts.

Figure 2 shows a distribution of events in the diagonal time projection of Fig. 1, $\tau \equiv 2t_e - t_{\gamma_1} - t_{\gamma_2}$. Only $\mu^+ \rightarrow e^+\gamma\gamma$ decays produce a peak in τ. Events shown in Fig. 2 have $|\tau| < 4.0$ ns, and so only 272 of the 364 events are displayed. No appreciable coincidence signal can be seen from this plot.

Conservation of momentum requires that a three-body decay at rest be coplanar and that the vector sum of the momenta in the decay plane equals zero. Two variables

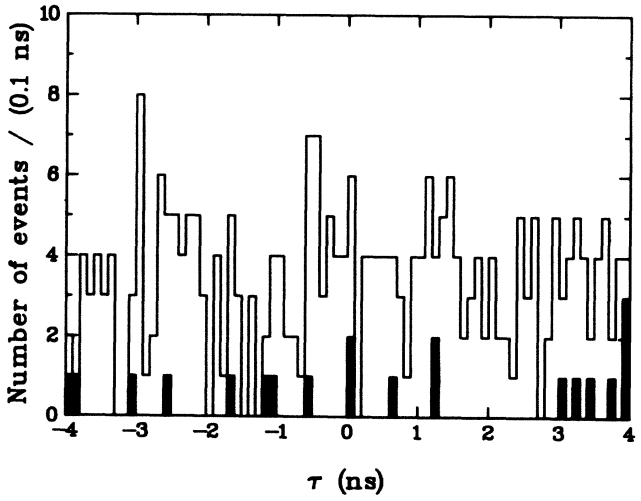

FIG. 2. Distribution of the final twenty data events (solid bars) in the diagonal time projection of Fig. 1. Superimposed on this plot is the distribution of 272 data events with relaxed cuts.

are defined to test momentum conservation. One variable is a momentum sum within the decay plane, $p_{\parallel} \equiv |\mathbf{p}_a + \mathbf{p}_b + \hat{\mathbf{p}}_{ab} \times (\mathbf{p} \times \hat{\mathbf{p}}_{ab})|$, where $\mathbf{p}_a$ and $\mathbf{p}_b$ are the momenta of the particles that are most nearly perpendicular to each other, $\hat{\mathbf{p}}_{ab}$ is the unit vector normal to the plane determined by $\mathbf{p}_a$ and $\mathbf{p}_b$, and $\mathbf{p}_c$ is the momentum vector of the third particle. The other variable is independent of the scale of the energy measurement and is $\cos\alpha \equiv \hat{\mathbf{p}}_c \cdot \hat{\mathbf{p}}_{ab}$. Events are required to satisfy $p_{\parallel} < 14$ MeV/c, $-0.2 \leq \cos\alpha < 0.2$, and $90 \leq E_T < 108$ MeV, where E_T is the sum of the three measured energies. Only twenty candidate events satisfy these requirements and 15.8% of any $\mu^+ \to e^+\gamma\gamma$ events would be discarded. The τ distribution of these twenty events is shown in Fig. 2 as solid bars. All remaining $\mu^+ \to e^+\gamma\gamma$ events should have $|\tau| < 2.5$ ns. There is no evidence for an excess of events with small values of $|\tau|$.

The maximum-likelihood method is used to estimate the number of $\mu^+ \to e^+\gamma\gamma$ events in the nine surviving events with $|\tau| < 2.5$ ns. The likelihood function is defined to be

$$L(n_{e\gamma\gamma}) = \prod_{i=1}^{N} \left[\frac{n_{e\gamma\gamma}}{N} Q(\mathbf{x}_i) + \frac{n_B}{N} R(\mathbf{x}_i) \right],$$

where N is the total number of events, $n_{e\gamma\gamma}$ is the estimate of the number of $\mu^+ \to e^+\gamma\gamma$ events, and $n_B = N - n_{e\gamma\gamma}$ is the estimate of the number of events due to backgrounds. The vector $\mathbf{x}$ has the components E_T, $p_{\parallel}$, $\cos\alpha$, and τ. The Q and R are the normalized probability distributions for $\mu^+ \to e^+\gamma\gamma$ and background events, respectively. The best estimates for $n_{e\gamma\gamma}$ and n_B are those values that maximize the likelihood function, for positive values of $n_{e\gamma\gamma}$ and n_B.

The Q probability distribution for $\mu^+ \to e^+\gamma\gamma$ events is generated by a Monte Carlo simulation. This program accurately reproduces the detector elements and their response, and uses the electromagnetic-shower code EGS3.[8] The Monte Carlo program uses the final-state particle momentum distributions[9] calculated from a general local interaction contributing to $\mu^+ \to e^+\gamma\gamma$. The probability distributions for the $\mu^+ \to e^+\gamma\gamma$ events are somewhat different for the three-quadrant events and the two-quadrant events. The R probability distribution for random background events is taken from data events with $2.5 < |\tau| < 5$ ns. The background probability distribution for τ is a constant value over the region of interest.

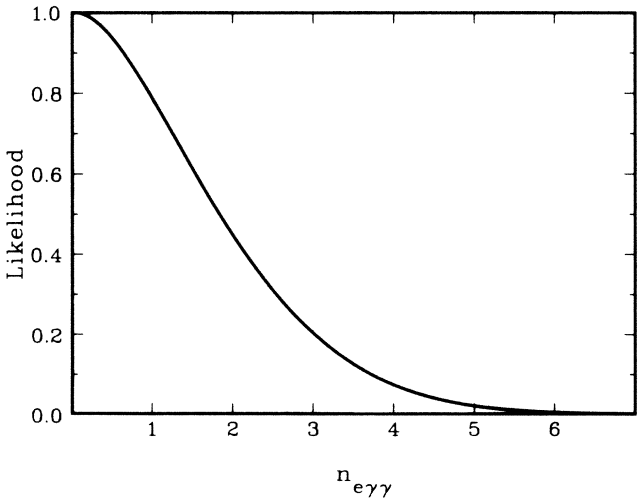

FIG. 3. The normalized likelihood function vs the number of $\mu^+ \to e^+\gamma\gamma$ events, $n_{e\gamma\gamma}$, for the nine data events.

The normalized likelihood function is shown in Fig. 3 for the nine surviving data events. The function peaks at $n_{e\gamma\gamma} = 0$, and the shape of the likelihood distribution gives $n_{e\gamma\gamma} \leq 2.9$ events (90% C.L.). This result is insensitive to reasonable variations in the probability distributions. The distributions of events in E_T, $p_{\parallel}$, $|\tau|$, and $\cos\alpha$ are each consistent with those expected for background events.

The number of muons stopped on the target during the live time of the experiment is 1.2×10^{12}. The detector acceptance for $\mu^+ \to e^+\gamma\gamma$ is 0.064, as determined from Monte Carlo simulation. The detection efficiency is 0.524 with the major losses coming from the definition of photons (uncorrelated positrons accidentally vetoing a photon) and from rejection of events with piled-up energies. Combining these numbers, we obtain

$$B_{\mu e\gamma\gamma} < 7.2 \times 10^{-11} \text{ (90\% C.L.)}.$$

This result is an improvement of more than 2 orders of magnitude over the previous limit. No evidence for lepton-family-number nonconservation is observed in this experiment.

A large number of people from our institutions have made this experiment possible, and we acknowledge their contributions in this effort. This work was supported in part by the U.S. Department of Energy and the National Science Foundation.

[a]Present address: Physics Department, Princeton University, Princeton, NJ 08544.

[b]Present address: Elektrowatt Ing. AG, Zurich, Switzerland.

[c]Present address: Lawrence Berkeley Laboratory, Berkeley, CA 94720.

[d]Present address: Swiss Institute for Nuclear Research, CH-5234 Villigen, Switzerland.

[e]Present address: Los Alamos National Laboratory, Los Alamos, NM 87545.

[f]Present address: Lockheed Missiles and Space Co., Palo Alto, CA 94304.

[1]S. L. Glashow, Nucl. Phys. **22**, 579 (1961); A. Salam, in *Elementary Particle Theory: Relativistic Groups and Ana-*

lyticity, Nobel Symposium No. 8, edited by N. Svartholm (Almqvist and Wiksell, Stockholm, 1968), p. 367; S. Weinberg, Phys. Rev. Lett. **19**, 1264 (1967).

[2]Y. Tomozawa, Phys. Rev. D **25**, 1448 (1982); V. Visnjić-Triantafillou, Phys. Lett. **95B**, 47 (1980).

[3]F. Wilczek and A. Zee, Phys. Rev. Lett. **38**, 531 (1977).

[4]J. D. Bowman, T. P. Cheng, L.-F. Li, and H. S. Matis, Phys. Rev. Lett. **41**, 442 (1978).

[5]G. Azuelos *et al.,* Phys. Rev. Lett. **51**, 164 (1983).

[6]R. D. Bolton *et al.,* Phys. Rev. Lett. **53**, 1415 (1984).

[7]R. D. Bolton *et al.,* Phys. Rev. Lett. **56**, 2461 (1986).

[8]R. L. Ford and W. R. Nelson, Stanford Linear Accelerator Center Report No. SLAC-PUB-210, 1978 (unpublished).

[9]J. Dreitlein and H. Primakoff, Phys. Rev. **126**, 375 (1962).